Materials Science in Semiconductor Processing ∎ (∎∎∎∎) ∎∎∎–∎∎∎

Contents lists available at ScienceDirect

Materials Science in Semiconductor Processing

journal homepage: www.elsevier.com/locate/mssp

Effect of sodium doping on graded $Cu(In_{1-x}Ga_x)Se_2$ thin films prepared by chemical spray pyrolysis

B.J. Babu [a,b], S. Velumani [a,*], Brian J. Simonds [c], Richard K. Ahrenkiel [d], A. Kassiba [b], R. Asomoza [a]

[a] Department of Electrical Engineering-SEES, CINVESTAV-IPN, Zacatenco, D. F., C.P 07360, Mexico
[b] Institute of Molecules and Materials, UMR-CNRS 6283, Universite du Maine, Avenue O. Messiaen, F-72085 Le Mans, France
[c] Department of Physics, Colorado School of Mines, Golden, CO 80401, United States
[d] Department of Metallurgical and Materials Engineering, Colorado School of Mines, Golden, CO 80401, United States

ARTICLE INFO

Keywords:
Graded CIGS layer
Na doping
TMPCD
Minority lifetime

ABSTRACT

In the present work we have studied the effect of Na on the properties of graded Cu $(In_{1-x}Ga_x)Se_2$ (CIGS) layer. Graded CIGS structures were prepared by chemical spray pyrolysis at a substrate temperature of 350 °C on soda lime glass. Sodium chloride is used as a dopant along with metal (Cu/In/Ga) chlorides and n, n-dimethyl selenourea precursors. The addition of Na exhibited better crystallinity with chalcopyrite phase and an improvement in preferential orientation along the (112) plane. Energy dispersive analysis of X-rays (line/point mapping) revealed a graded nature of the film and percentage incorporation of Na (0.86 at%). Raman studies showed that the film without sodium doping consists of mixed phase of chalcopyrite and CuAu ordering. Influence of sodium showed a remarkable decrease in electrical resistivity (0.49–0.087 Ω cm) as well as an increase in carrier concentration (3.0×10^{18}–2.5×10^{19} cm^{-3}) compared to the un-doped films. As carrier concentration increased after sodium doping, the band gap shifted from 1.32 eV to 1.20 eV. Activation energies for un-doped and Na doped films from modified Arrhenius plot were calculated to be 0.49 eV and 0.20 eV, respectively. Extremely short carrier lifetimes in the CIGS thin films were measured by a novel, non-destructive, noncontact method (transmission modulated photoconductive decay). Minority carrier lifetimes of graded CIGS layers without and with external Na doping are found to be 3.0 and 5.6 ns, respectively.

1. Introduction

$Cu(In_{1-x}Ga_x)Se_2$ (CIGS) thin film solar cells with an active area of 0.5 cm^2 fabricated by researchers at Stuttgart's Centre for Solar Energy and Hydrogen Research (ZSW) exhibited a record efficiency of 21.7% [1]. Cu_xS/CdS thin film solar cells seem to be the origin for the development of CIGS thin film solar cells in which Cu_xS is an unstable compound with time [2]. In order to improve stability of the compound, indium is added to it to make strong covalent bonding that turns into $CuInS_2$. $CuInSe_2$ (CIS), $CuGaSe_2$ (CGS), and $CuAlSe_2$ are derivative compounds of $CuInS_2$ [3]. The theoretical models reveal that 1.55 eV band gap absorber materials are optimal to capture maximum solar spectrum [3,4]. Based on this, $CuInS_2$ is a suitable material but its performance is inferior to $CuInSe_2$. The band gap of $CuInSe_2$ is 1.1 eV [3,5] therefore band gap needs to be increased by adding either Ga or Al in it [6].

The quaternary CIGS system allows the band gap of the semiconductor to be adjusted over a range of 1.04–1.67 eV [7]. Using a non-uniform Ga/In ratio throughout the film thickness, band gap grading can be achieved. Numerical

* Corresponding author. Tel.: +52 55 5747 4001; fax: +52 55 5747 4003.
E-mail address: velu@cinvestav.mx (S. Velumani).

http://dx.doi.org/10.1016/j.mssp.2015.01.002
1369-8001/© 2015 Published by Elsevier Ltd.

modeling tools are used to show the beneficial effect of grading. Back grading in CIGS solar cells improves simulated device efficiency compared to ungraded devices [8]. For devices with standard thicknesses, the effect is small, around 0.5% in efficiency. The potential efficiency gain increases significantly as the absorber thickness is reduced [8,9]. Lundberg et al. [9] claimed that fill factor loss was eliminated by introducing a Ga/(Ga+In) graded CIGS, which also resulted in an increased open-circuit voltage of 20–30 mV for a thin (0.8 μm) absorber layer.

The most important effect of soda lime glass substrate on CIGS film growth is that it supplies sodium to growing chalcopyrite material. Sodium incorporated into CIGS absorber layers are widely known to have significant beneficial effects that lead to enhanced CIGS-related photovoltaic cell efficiencies. Two main phenomenological effects have been found to result from Na incorporation: (i) an improvement in *p*-type conductivity due to an increase in the effective hole carrier density and improved open circuit voltage (V_{oc}) and fill factor for solar cells fabricated from Na doped CIGS [10] and (ii) enhancement of (112) orientation for films grown with Na doping [11]. Effect of sodium doping, Cu/(In+Ga) and Ga/(In+Ga) ratios on efficiency of superstrate solar cell was examined by Nakada et al. [12].

Minority carrier lifetime is an important parameter in discerning the quality of solar cell absorber materials. It is difficult to measure carrier lifetime of thin film materials because of shorter decay lifetimes. For measuring minority-carrier lifetime in semiconductor materials number of contactless techniques are available such as microwave photoconductivity decay (μPCD) [13], resonant coupled photoconductivity decay (RCPCD) [14], transmission modulated photoconductive decay (TMPCD) [15,16], Quasi-steady state photoconductivity (QSSPC) [17] and time-resolved photoluminescence (TRPL) [18–20]. TMPCD is a newly developed technique which appears to have high enough sensitivity and time resolution to measure the extremely short carrier lifetimes on the order of a nanosecond [16].

Usually grading of CIGS layer is achieved by a three-stage co-evaporation process [21–23]. In our lab CIGS nanopowders and thin films are fabricated by non-vacuum processes such as mechano-chemical alloying [24–26] and screen-printing [25], spray pyrolysis [27,28], respectively. Here, for first time, we prepared graded CIGS layers using a spray pyrolysis technique. Influence of sodium doping on structural, electrical and optical properties of graded CIGS thin films deposited by spray pyrolysis are discussed. We used μPCD, RCPCD and TMPCD to measure minority carrier life time of graded CIGS layers. These films produced no signals either in μPCD or RCPCD, showing TMPCD is capable of measuring shorter lifetime. Though the lifetime of CIGS films was determined by TRPL [19,20], this is the first attempt to report the shortest lifetime of graded CIGS layers measured by TMPCD.

2. Experimental details

Graded CIGS thin films were prepared by chemical spray pyrolysis using 20 vol% aqueous ethanol (Fermont) solution containing copper chloride ($CuCl_2 \cdot 2H_2O$), indium tri chloride ($InCl_3$), gallium tri chloride ($GaCl_3$) and n, n dimethyl selenourea ($C_3H_8N_2Se$) (all are annular grade from Aldrich, USA) as the starting solutions. Concentrations of $CuCl_2$ and $GaCl_3/InCl_3$ were maintained at 0.0015 M while that of selenourea was 0.0055 M. Cu:(Ga+In):Se atomic ratio in the solution was maintained as 1:1:3.5. An excess of n, n dimethyl selenourea was taken in the starting solution in order to complete the reaction and compensate the loss of selenium during deposition due to its high vapor pressure. The relative concentrations of $GaCl_3$ and $InCl_3$ were varied appropriately to achieve the desired x=Ga/(Ga+In) ratio in the films while their total concentration in the solution was kept constant. The solutions were sprayed onto soda–lime glass substrates maintained at a temperature of 350 °C with an accuracy of ±1 °C measured using Shinko model JCS-33A-S/M temperature controller. The solution was sprayed at a flow rate of 6.5 ml/min. Nitrogen was used as the carrier gas at a flow rate of ~15–20 psi. The source to substrate distance was maintained as 25 cm. The entire deposition process was carried out taking solution in dark container and also in the absence of electrical light inside the deposition chamber to avoid the dissociation of selenourea into elemental selenium. Two different kinds of stacking with and without sodium doping layers (4 samples, namely G1($x \rightarrow 0$ to 1), G1_Na, G2($x \rightarrow 1$ to 0) and G2_Na) were deposited as shown in Fig. 1. In 385 ml of Cu(In, Ga)Se_2 solution, 0.12 mg of sodium chloride (NaCl) (SigmaAldrich, 99.99% pure) salt is added in order to dope sodium externally. The time of deposition of total CIGS layer was 125 min (25 min × 5 layers, each layer with different x value).

Structural characterization of deposited CIGS films was carried out using a PANalytical Xpert X-Ray Diffractometer with CuKα_1 (λ=1.5406 Å) in the θ–2θ mode. XRD spectra were recorded in the scanning range 20–60°. Raman dispersion studies were made in a Horiba-Jobin Yvon equipment, model LabRAM HR800 with He–Ne laser operated at 632 nm of 20 mW. In order to avoid heating of the sample and to filter plasma frequencies a D0.6 filter was employed which reduces power to 5 mW. Surface morphology of the films was examined by Carl Zeiss AURIGA field emission scanning electron microscopy (FESEM) workstation. Compositions of all the deposited films were determined using a Bruker energy dispersive analysis of X-ray (EDAX) system attached to a secondary electron microscope. Optical absorption spectra of CIGS thin films have been recorded as a function of wavelength in the range between 400 and 2000 nm by a Cary 5G UV–vis–NIR spectrophotometer. Hall measurements were carried out by the Van der Pauw method using a Walker scientific HV-4H equipment. Temperature dependence *I*–*V* characteristics of CIGS thin films were examined using a Keithley 6487 picoammeter/voltage source and Lakeshore 330 auto-tuning temperature controller between 25 and 125 °C. We measured carrier lifetime of graded CIGS thin films using a novel, non-destructive, noncontact method (TMPCD). A RF signal with a frequency of 500 MHz is transmitted through sample, which bridges between transmitting and receiving coils. A pulsed laser beam operating at a wavelength of 532 nm with a pulse width of 4.3 ns is used to attenuate the RF conductivity in the sample. Minority carrier lifetime (τ_1) of CIGS layers is quantified by single exponential fitting to semi-log plot of rectified receiver output voltage versus time.

Please cite this article as: B.J. Babu, et al., Materials Science in Semiconductor Processing (2015), http://dx.doi.org/10.1016/j.mssp.2015.01.002

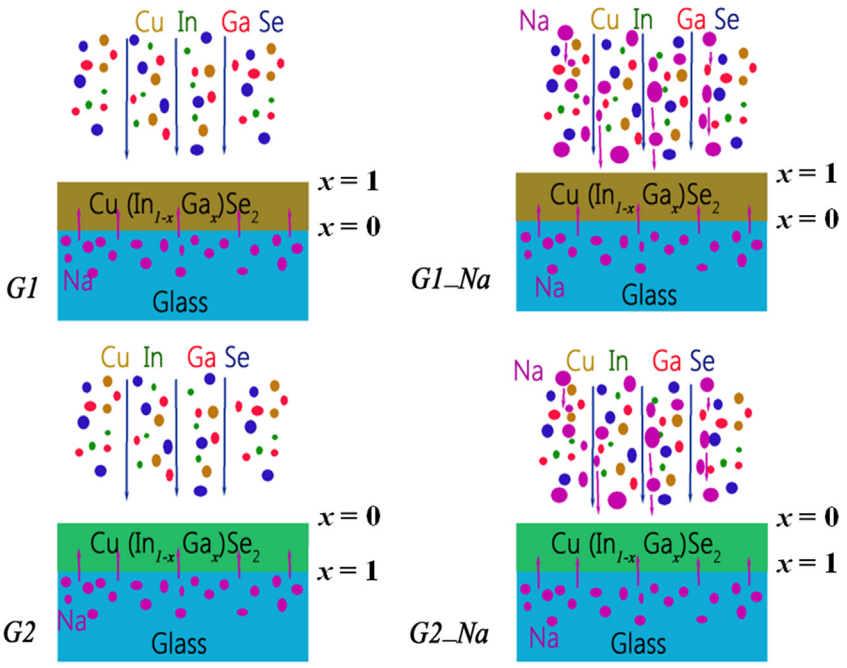

Fig. 1. Schematic diagram of graded CIGS thin film samples.

3. Results and discussion

XRD plot shown in Fig. 2, revealed that all the CIGS films were polycrystalline with a strong preferred orientation along (1 1 2) plane followed by weaker reflections from (2 2 0) and (1 1 6) planes [28–30]. In addition to these lattice planes, one weaker peak corresponding to (103) plane was also seen in the G2 film which is characteristic peak of chalcopyrite phase [31]. An inset of Fig. 2 depicts splitting of (220)/(204) and (312)/(116) in G1, which is good sign of chalcopyrite structure [7,24,32–33]. Structural parameters given in Table 1 illustrate the influence of sodium doping on crystallite size. Crystallite size of un-doped sample is slightly smaller compared to that of sodium doped CIGS film. From Table 2 the most obvious feature is the dominant (112) peak, in the case of films with external Na doping. Preferred orientation is controlled by Na impurities [10–11,34]. The {112} family of planes corresponds to the Cu and In lattice (Se excluded), it is intuitive that the "annihilation" of In_{Cu} antisites will lead to better ordering of the cations. Such ordering will result in an increase in the periodicity of {112} family of planes and therefore stronger diffraction intensity ("better crystallinity") is observed [10]. Lattice parameters were unchanged by the influence of Na doping and the films showed high degree of tetragonal ($c/a=2$) nature [32].

Raman studies given in Fig. 3 show a peak corresponding to A1 mode CIGS phase at 170 cm^{-1} for all the films except for G1_Na sample ($\sim$168 cm^{-1}) due to its lower gallium content [35]. Sample G2 showed the A1 mode with an asymmetric shape, and there seems to be a shoulder at higher frequency side. It is known that CIGS films grown using spray pyrolysis usually grow with mixed phase of chalcopyrite (CH) ordering and CuAu (CA) ordering [32], where the A1 peak of CH and CA ordering is located at $\sim$170 cm^{-1} and at $\sim$178 cm^{-1} respectively. For improvement of film quality, higher substrate temperature may be desirable as it is reported for the growth of $Cu(InGa)Se_2$ [7]. However, we had some difficulties related to growth rate in growing spray pyrolytic CIGS films at higher temperatures. Growth rate decreased from 19.44 to 2 nm, when the substrate temperature is increased from 350 to 400 °C due to re-evaporation of precursors. No other peaks corresponding to CuSe phase or any secondary phase were present in the Raman spectrum.

FESEM studies reveal that the CIGS thin films deposited onto soda–lime glass substrates at substrate temperature of 350 °C show different morphologies depending on gallium concentration on the top surface and external sodium doping as shown in Fig. 4. Sample G1 containing more gallium (CGS) on the top surface shows round grains, whereas G2 deposited with more indium (CIS) on top layer exhibit facets. External sodium doping influenced fusion and fission of grain structure in G1 and G2, respectively. Since G1 and G2 consist of different compositions their morphological changes with Na doping are also different. It is clear that sodium acted as fluxing agent and enhanced grain size in G1 [11]. On the other hand it decreased grain size by reducing hillock-like defects in G2. Reduction of grain sizes with increase in Na sodium content has been reported by Rudmann et al. [36]. Nevertheless this change is dependent on the doping concentration, method of deposition and composition of the film. However effect of sodium on grain sizes is not clear from the literature: an increase [10,11] and a decrease [36] along with the Na content are both reported.

Fig. 5 illustrates point and line mapping of G1 and G1_Na samples respectively. Point analyses showed that gallium concentration increased with an increase in layer thickness. Similarly line mapping depicts an intersection of indium and

Please cite this article as: B.J. Babu, et al., Materials Science in Semiconductor Processing (2015), http://dx.doi.org/10.1016/j.mssp.2015.01.002

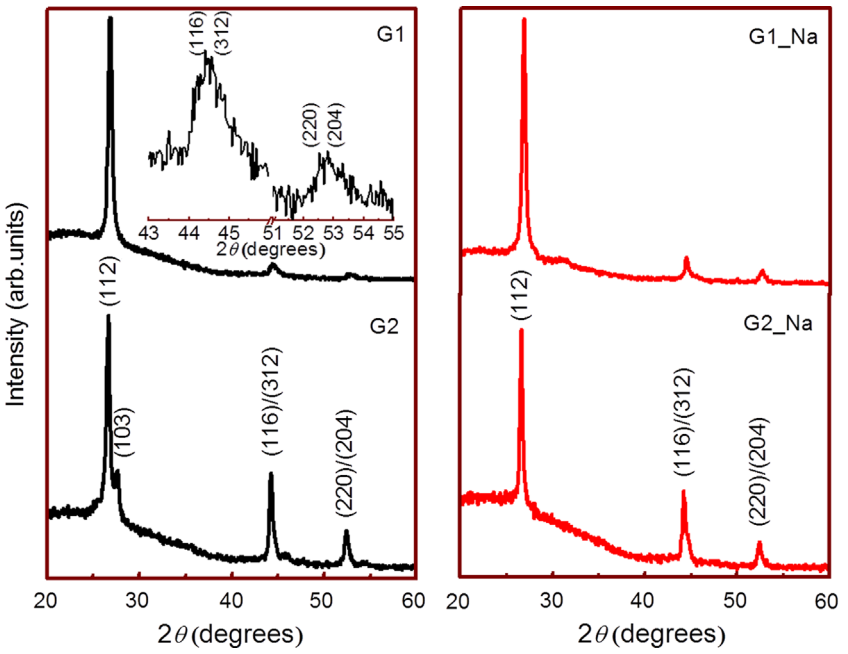

Fig. 2. XRD pattern of stacked $Cu(In_{1-x}Ga_x)Se_2$ layer with $x \rightarrow 0$ to 1(G1) and $x \rightarrow 1$ to 0 (G2), their sodium doping (G1_Na) and (G2_Na), respectively. An inset showing selected angle XRD pattern of G1.

Table 1
Structural parameters of graded un-doped (G1, G2) and Na-doped (G1_Na, G2_Na) CIGS thin films.

Sample CIGS	2θ (°)	FWHM, β (°)	Crystallite size, D (nm)
G1	26.84	0.55	15.42
G1_Na	26.86	0.49	17.31
G2	26.64	0.59	14.37
G2_Na	26.64	0.56	15.14

Table 2
Lattice parameters and texture coefficient of graded un-doped (G1, G2) and Na-doped (G1_Na, G2_Na) CIGS thin films.

Sample CIGS	a (Å)	c (Å)	c/a	Texture coefficient		
				(112)	(220)	(116)
G1	5.76	11.56	2.00	2.08	0.37	0.54
G1_Na	5.76	11.54	2.00	2.15	0.38	0.46
G2	5.78	11.83	2.04	1.25	0.84	0.90
G2_Na	5.78	11.83	2.04	1.32	0.80	0.87

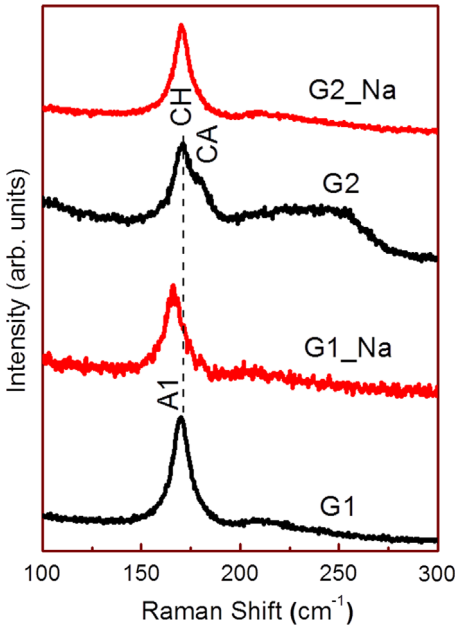

Fig. 3. Raman spectra of graded un-doped (G1, G2) and Na-doped (G1_Na, G2_Na) CIGS thin films.

gallium atomic percentages revealing the graded nature of the films. Line mapping of G2 and G2_Na samples is given in Fig. 6, the Ga/(In+Ga) decreased rapidly from 0.67 to 0.20, suggesting the formation of a graded band gap CIGS absorber layer. External sodium doping of G1_Na and G2_Na was determined using EDAX and the value obtained is 0.8 at%, here sodium due to internal diffusion from the glass substrate is subtracted. Cu/(In+Ga) ratio varies from 0.77 to 1.06 from bottom to top layer. Grading of the Ga/(In+Ga) atomic ratio was intentionally formed by controlling Ga and In concentrations in the solutions during CIGS deposition. The beneficial effect of such grading on conversion efficiency (19.2%) of CIGS thin film solar cell has been addressed by Ramanathan et al. [21].

Fig. 7(a) shows absorption spectra of graded CIGS thin films without and with Na doping. Optical band gap of these films was extracted from $(\alpha h\nu)^2$ versus $(h\nu)$ graphs as presented in Fig. 7(b)–(e). The deviation in the band gap of G1 (1.32 eV) and G2 (1.20 eV) is due to the difference in average gallium concentration in the films. As carrier concentration in

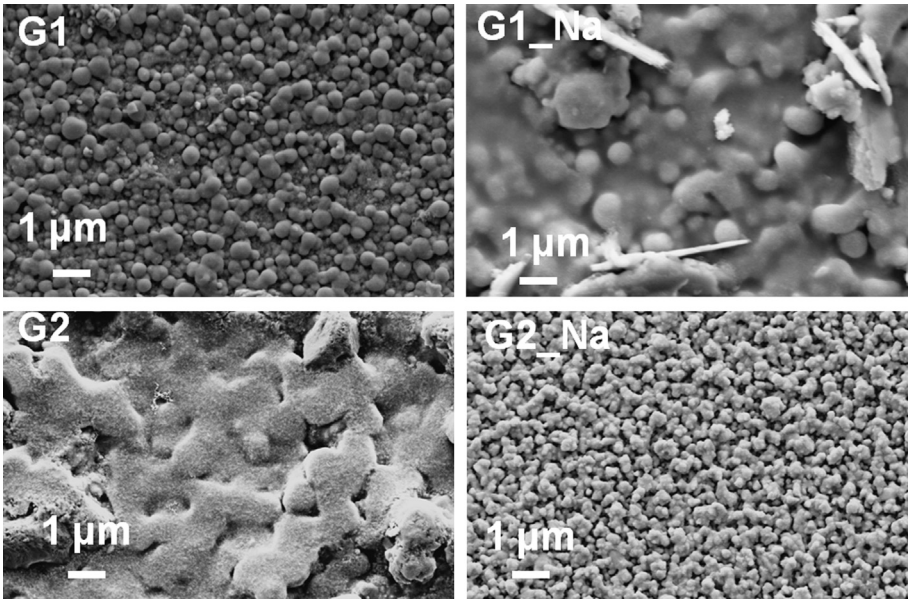

Fig. 4. FESEM images of graded un-doped (G1, G2) and Na-doped (G1_Na, G2_Na) CIGS layer.

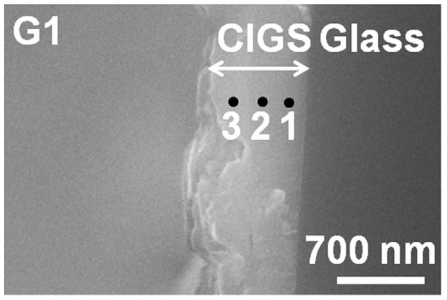

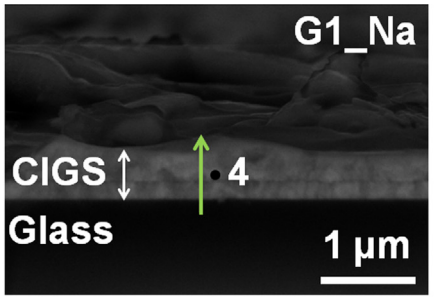

Location	Cu (at.%)	In (at.%)	Ga (at.%)	Se (at.%)
		G1		
Point 1	30.41	13.36	5.49	50.24
Point 2	31.26	9.72	13.05	45.97
Point 3	36.10	9.20	13.09	41.62
		G1_Na		
Point 4	24.46	14.45	10.64	50.45
Point 4		Na = 0.83 at.%		

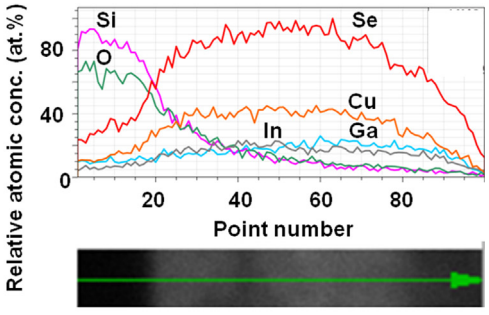

Fig. 5. Point analysis and line mapping of graded un-doped CIGS (G1) and Na-doped CIGS (G1_Na) layer.

the G1 film increased after sodium doping, band gap shifted from 1.32 eV (Fig. 7(b)) to 1.20 eV (Fig. 7(c)), similarly in the case of G2 film it shifted from 1.20 eV (Fig. 7(d)) to 1.17 eV (Fig. 7(e)). In heavily doped *n*-type semiconductors, the absorption edge lies at much shorter wavelengths as compared to the intrinsic case. For *p*-type semiconductors, the absorption thresholds occur in the opposite order [33,37]. This effect, known as the Moss–Burnstein shift, is depicted in Fig. 7(a) for CIGS: Na films with different carrier concentrations.

Table 3 represents resistivity (ρ), mobility (μ) and carrier concentration (p) of graded CIGS thin films with respect to sodium doping. The most obvious electronic effect of Na incorporation into CIGS films as measured by the Hall Effect is a decrease in resistivity by up to two orders of magnitude and increase in carrier concentration [38] as given in Table 3. Mobility of G2_Na sample is decreased compared to G1_Na probably due to increase in grain boundary scattering of carriers because of smaller grain sizes as given in Table 1 and surface morphologies shown in Fig. 4. According to Contreras et al. [10] mobility values do not seem to be significantly affected by the impurities (Na, K, Cs) and are usually in the 1–10 $cm^2/V\,s$ range. The effect of Na includes an improvement in *p*-type conductivity due to an increase in the effective hole carrier density and improved open circuit

Please cite this article as: B.J. Babu, et al., Materials Science in Semiconductor Processing (2015), http://dx.doi.org/10.1016/j.mssp.2015.01.002

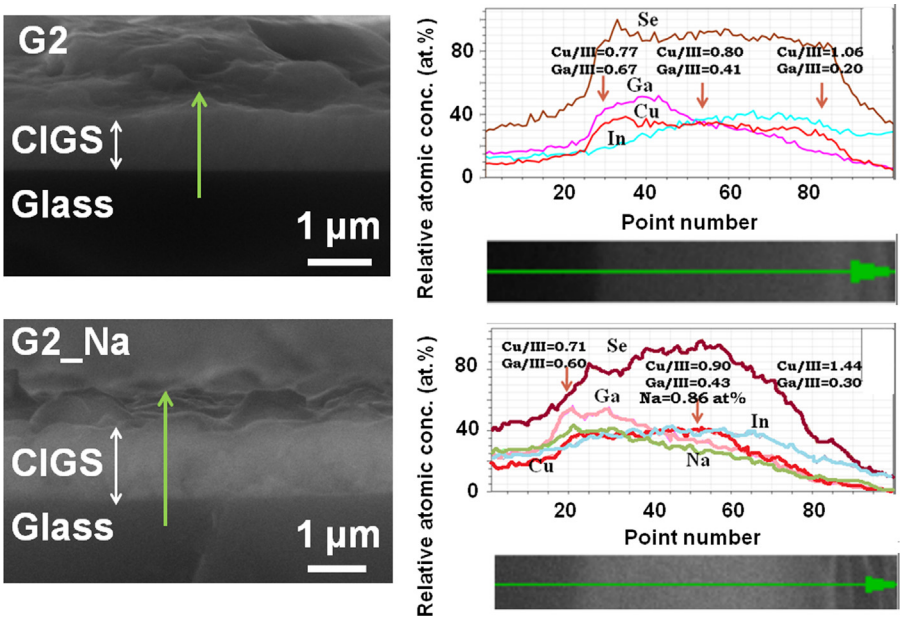

Fig. 6. Line mapping of graded un-doped CIGS (G2) and Na doped CIGS (G2_Na) layers.

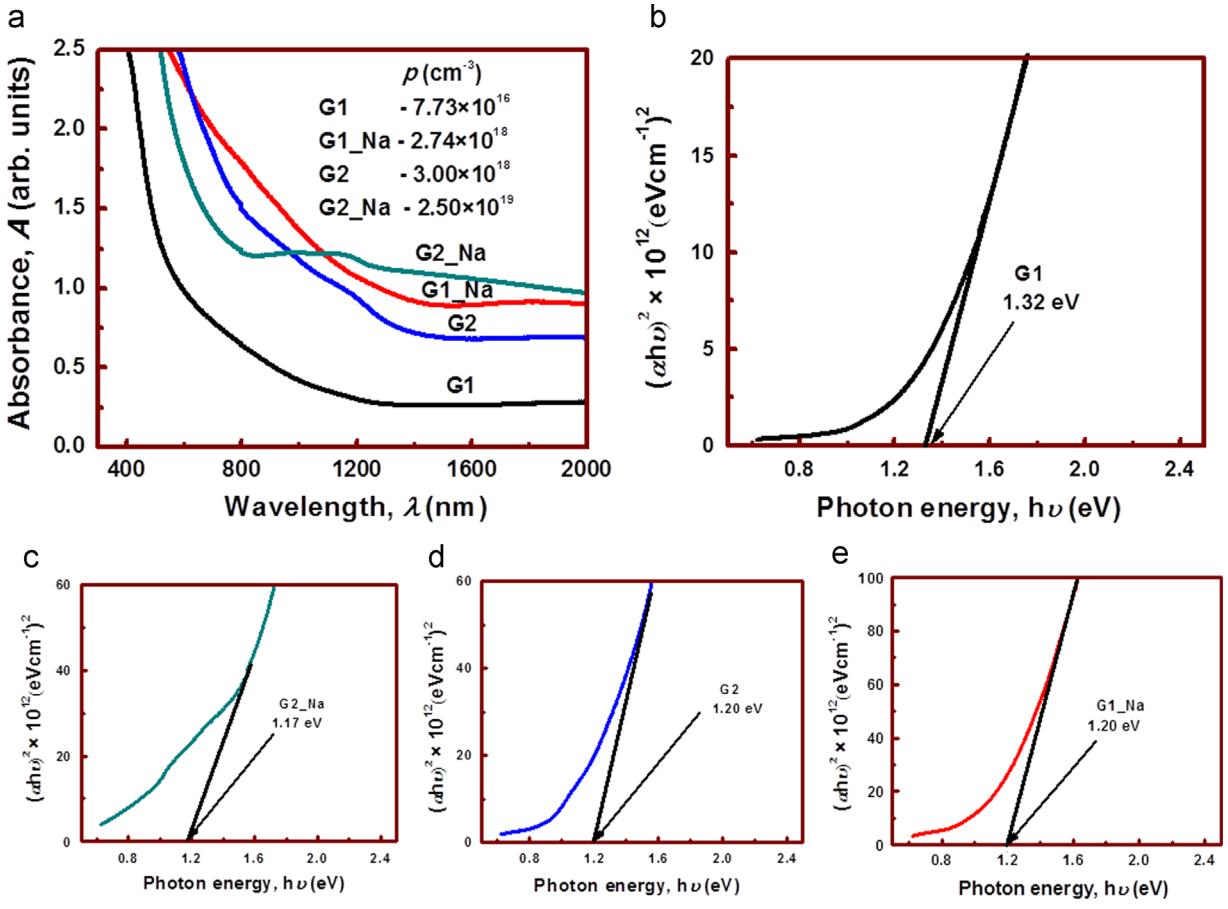

Fig. 7. (a) Absorbance spectra of graded un-doped (G1, G2) and Na-doped (G1_Na, G2_Na) CIGS layers, (b), (c), (d) and (e) $(\alpha h\nu)^2$ versus $h\nu$ graphs for G1, G1_Na, G2 and G2_Na respectively.

Please cite this article as: B.J. Babu, et al., Materials Science in Semiconductor Processing (2015), http://dx.doi.org/10.1016/j.mssp.2015.01.002

voltage (V_{oc}) and fill factor for solar cells fabricated from Na doped CIGS [34,38].

Sodium addition increased carrier concentration in CIGS due to incorporation of Na onto In or Ga lattice sites, where it would directly act as an acceptor, or due to reduction of compensating $(In, Ga)_{Cu}$ defects (In or Ga atom on Cu site) by substitution with Na_{Cu} [10]. Stanbery et al. [39] proposed that Na acts as a surfactant during the growth of CIS by destabilizing $(2V_{Cu}+In_{Cu})$ neutral defect complexes in the near-surface region, and thereby reducing the amount of In_{Cu} compensating donors and enhancing the crystal quality [10,39]. Rudmann [40] proposed that the main electronic action of Na is the passivation of defects such as hole traps at the grain boundaries, which can remove recombination centers, modify barrier heights and depletion widths around the grain boundaries, and which leads to increased effective carrier concentration and minority carrier diffusion length.

Table 3
Resistivity (ρ), mobility (μ) and carrier concentration (p) of graded un-doped (G1, G2) and Na-doped (G1_Na, G2_Na) CIGS thin films with respect to sodium doping.

Sample CIGS	Resistivity, ρ (Ω cm)	Mobility, μ (cm^2/V s)	Concentration, p (cm^{-3})
G1	20.06	4.02	7.73×10^{16}
G1_Na	0.155	14.63	2.74×10^{18}
G2	0.490	4.20	3.00×10^{18}
G2_Na	0.087	2.85	2.50×10^{19}

Fig. 8 presents temperature dependent *I–V* characteristics of graded un-doped (G1, G2) and Na-doped (G2_Na) CIGS thin films. The curves at low temperatures are distorted and showed ohmic nature as temperature increased. With sodium doping, the layers showed no distortion and reported high current compared to un-doped film. In order to determine the activation energy (E_A), a modified Arrhenius plot is used as shown in Fig. 9. Log (I) is plotted versus the inverse thermal voltage ($1/kT$) at 10 V for G1, G2 and 1 V for G1_Na, as given in the following equation:

$$\log_{10} I = \log_{10} I_0 - (E_A/kT) \quad (1)$$

Here I_0 denotes the saturation current pre-factor is relatively constant with respect to temperature. CIGS thin film with G1 and G2 configuration showed activation energy of 0.46 eV and 0.49 eV, respectively as shown in

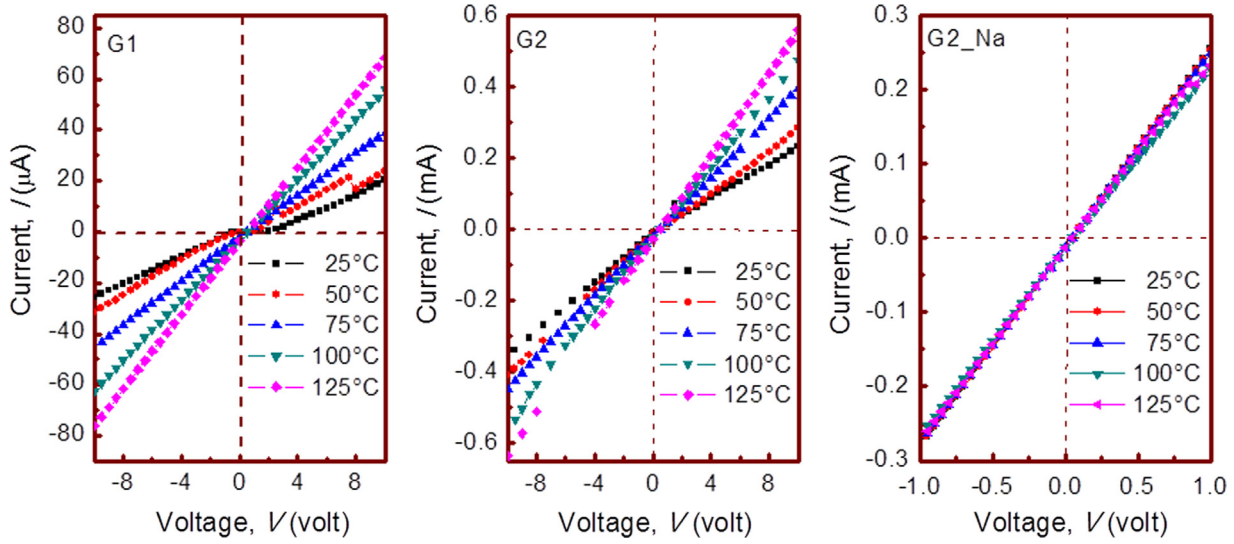

Fig. 8. Temperature dependent *I–V* characteristics of graded un-doped (G1, G2) and Na-doped (G2_Na) CIGS thin films.

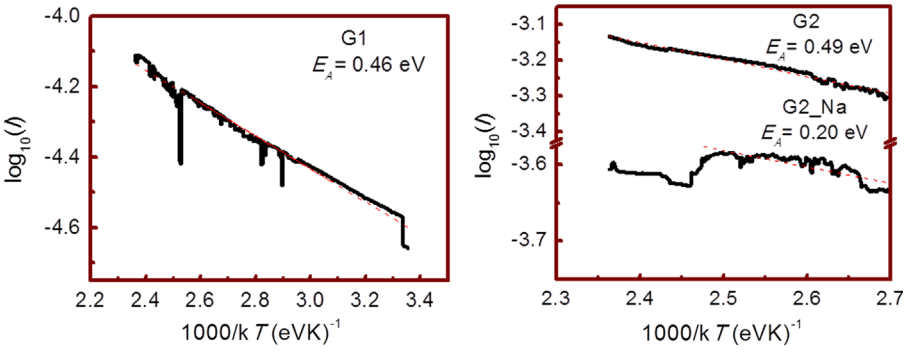

Fig. 9. Modified Arrhenius plots of current versus temperature, with their linear fit curves for graded un-doped (G1, G2) and Na-doped (G2_Na) CIGS thin films.

Please cite this article as: B.J. Babu, et al., Materials Science in Semiconductor Processing (2015), http://dx.doi.org/10.1016/j.mssp.2015.01.002

Fig. 9, which are related to donor like trap (conduction band, E_c −0.46 eV) [33]. The activation energy of ZnO/CIGS junction was reported as 0.5 eV by Haug et al. [41] which agrees with our results quite well. Upon sodium addition to G2 sample the activation energy decreased by 290 meV. Reduced band bending resulting from a higher than desirable activation energy of the CIGS film could be one of the reason for unexceptional V_{oc} of devices.

The vast majority of photoconductive or PL decay curves on CIGS films and devices can be fit well with a bi-exponential function as given in following equation:

$$I_{PL}(t) = C_1 \exp\ (-t/\tau_1) + C_2 \exp\ (-t/\tau_2) \quad (2)$$

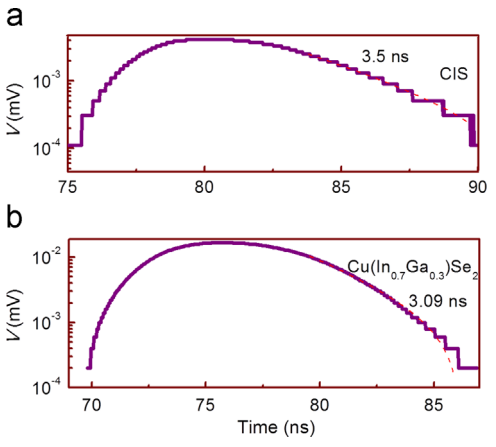

Fig. 10. TMPCD response of (a) CIS and (b) CIGS layers on a glass substrate. The data were obtained using 532 nm pulsed excitation.

where C_1 and C_2 are coefficients, and τ_1 and τ_2 are decay times that correspond to the low and high injections regions of the decay curves, respectively. However, in our case lifetime (τ_1) of CIS and CIGS layers are quantified by a single exponential fitting to semi-log plot of rectified receiver output voltage versus time as illustrated in Fig. 10(a) and (b). The minority carrier lifetime of CIS and CIGS layers was 3.5 and 3.09 ns respectively. Reported values for τ_1 on CIGS films and solar cells measured by TRPL under very different injection conditions have ranged from several hundred nanoseconds to single nanoseconds [19,20]. Metzger et al. [19] observed lifetime of 250 ns for as-deposited CIGS films, which then reduced to 1 ns for one day exposure to air. It is also seen that these as deposited films showed similar lifetimes after CdS layer deposition on them, indicating that the deposition of CdS or other buffer layers passivates the CIGS film surface. Shirakata et al. [20] showed typical lifetime of 2–10 ns for CIGS solar cells and that of film was 0.7–3 ns.

We also extracted minority carrier lifetime on graded un-doped (G1, G2) and Na-doped (G1_Na, G2_Na) CIGS thin films and found to be 3.0, 3.45 and 5.6, 4.67 ns, respectively, as illustrated in Fig. 11(a) and (b). An increase in the lifetime of sodium doped CIGS film may be related to increase in carrier concentration as given in Table 3. Though our films reported lower life time as compared with high efficiency CIGS devices [19], it is very much comparable (5.4 ns) with 15.2% CIGS thin film device developed by using a non-vacuum hydrazine based process [42]. Range of allowed carrier lifetimes determines diffusion length in an absorber layer of a solar cell device. Let us consider diffusion coefficient, $D=\mu(kT/q)$ and diffusion length, $L=(D\times\tau)^{1/2}$.

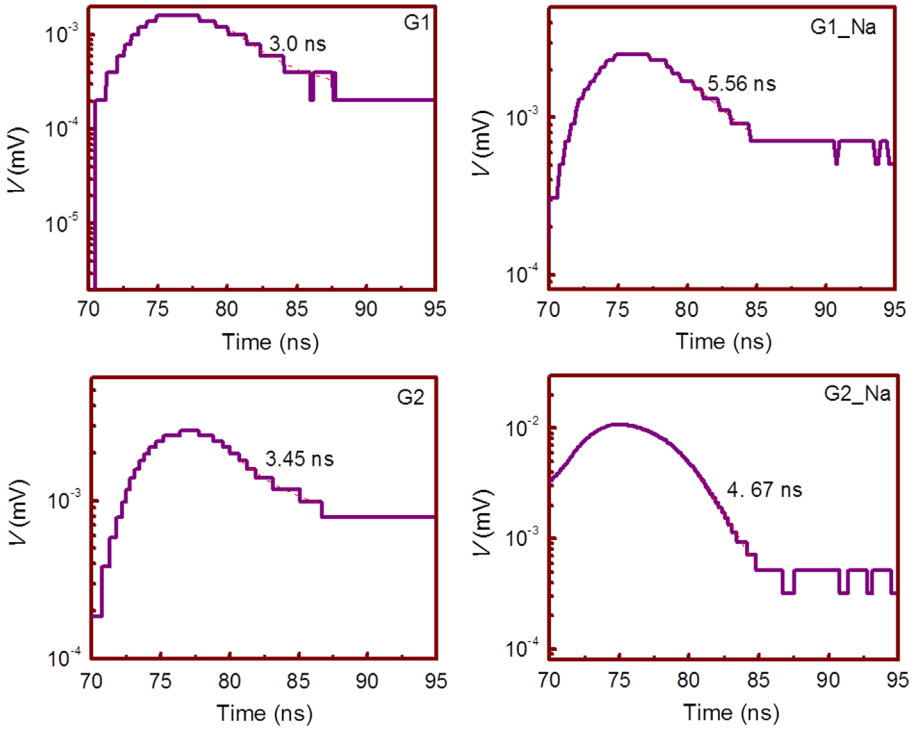

Fig. 11. TMPCD response of graded un-doped (G1, G2) and Na-doped (G1_Na, G2_Na) CIGS layers on a glass substrate. The data were obtained using 532 nm pulsed excitation.

Please cite this article as: B.J. Babu, et al., Materials Science in Semiconductor Processing (2015), http://dx.doi.org/10.1016/j.mssp.2015.01.002

If $\tau=3$ ns and mobility (μ) is 4 $cm^2/V\,s$ then at 300 K, $L=0.176$ μm. So diffusion length must be of the order of the absorption length when diffusion is being used for the transport of photogenerated minority carriers out of the absorber region.

4. Conclusions

CIGS thin films with a graded structure were deposited using spray pyrolysis by varying the Ga/(In+Ga) ratio throughout the film. Point analyses showed that gallium concentration increased with increases in layer thickness. Graded CIGS structures showed characteristic peaks of chalcopyrite structure with preferred orientation along (112) plane. Minority carrier lifetime was measured to be 3 ns using TMPCD. Influence of external sodium in the graded structure was studied. Sodium doping (0.8 at%) enhanced preferred orientation along (112) plane by increase the crystallite size. The most obvious electronic effect of Na incorporation into CIGS films is decrease in resistivity by up to two orders and an increase in carrier concentration by one order of magnitude. An activation energy decreases by 290 meV upon sodium incorporation into graded CIGS structure. From photoconductive studies, the minority carrier lifetime was determined and found to increase (5.56 ns) with sodium doping due to increase in carrier concentration. We conclude that graded CIGS thin films deposited by pneumatic spray pyrolysis with external sodium doping showed good crystallinity and better electrical properties.

Acknowledgment

Authors thank Miguel Galván A (Raman studies) and Adolfo Tavira Fuentes (XRD studies) for their technical assistance. Our special thanks to Dr. Alejandro Avila for providing *I–V* measurement equipment. B. J. Babu is thankful to CONACyT for their continuous financial support to pursue Ph. D in Mexico.

References

[1] Press release dated 22nd September 2014. ⟨http://www.pv-magazine.com/news/details/beitrag/zsw-sets-217-thin-film-efficiency-record_100016505/#axzz3IAXN9AUl⟩, 2014 (accessed 24.11.14).
[2] D.C. Reynolds, G. Leies, L.L. Antes, R.E. Marburger, Phys. Rev. 96 (1954) 533–534.
[3] K.L. Chopra, P.D. Paulson, V. Dutta, Prog. Photovolt. Res. Appl. 12 (2004) 69–92.
[4] J.J. Loferski, J. Appl. Phys. 27 (1956) 777–784.
[5] T. Terasako, S. Inoue, T. Kariya, S. Shirakata, Sol. Energy Mater. Sol. Cells 91 (2007) 1152–1159.
[6] E. Halgand, J.C. Bernede, S. Marsillac, J. Kessler, Thin Solid Films 480-481 (2005) 443–446.
[7] S. Shirakata, Y. Kannaka, H. Hasegawa, T. Kariya, S. Isomura, Jpn. J. Appl. Phys. 38 (1) (1999) 4997–5002. (No. 9A).
[8] M. Gloeckler, J.R. Sites, J. Phys. Chem. Solids 66 (2005) 1891–1894.
[9] O. Lundberg, M. Bodegard, J. Malmstrom, L. Stolt, Prog. Photovolt. Res. Appl. 11 (2003) 77–88.
[10] M.A. Contreras, B. Egaas, P. Dippo, J. Webb, J. Granata, K. Ramanathan, S. Asher, A. Swartzlander, R. Noufi, in: Proceedings of the 26th IEEE PVSC, 1997, 359–362.
[11] P.S. Vasekar, N.G. Dhere, Sol. Energy Mater. Sol. Cells 93 (2009) 69–73.
[12] T. Nakada, T. Mise, in: Proceedings of the 17th European Photovoltaic Solar Energy Conference, 2001.
[13] M. Kunst, G. Beck, J. Appl. Phys. 63 (1988) 1093–1098.
[14] R.K. Ahrenkiel, S.W. Johnston, Mater. Sci. Eng. B 102 (2003) 161–172.
[15] R.K. Ahrenkiel, D.J. Dunlavy, Sol. Energy Mater. Sol. Cells 95 (2011) 1985–1989.
[16] B.J. Simonds, B. Yan, G. Yue, D.J. Dunlavy, R.K. Ahrenkiel, P.C. Taylor, Mater. Res. Soc. Symp. Proc. 1245 (2010).
[17] R.A. Sinton, A. Cuevas, Appl. Phys. Lett. 69 (17) (1996) 2510–2512.
[18] R.K. Ahrenkiel, Solid-State Electron. 35 (3) (1992) 239–250.
[19] W.K. Metzger, I.L. Repins, M.A. Contreras, Appl. Phys. Lett. 93 (2008) 022110-1–022110-3.
[20] S. Shirakata, T. Nakada, Thin Solid Films 515 (2007) 6151–6154.
[21] K. Ramanathan, M.A. Contreras, C.L. Perkins, S. Asher, F.S. Hasoon, J. Keane, D. Young, M. Romero, W. Metzger, R. Noufi, J. Ward, A. Duda, Prog. Photovolt. Res. Appl. 11 (2003) 225–230.
[22] J. Sastre-Hernandez, M.E. Calixto, M. Tufino-Velazquez, G. Contreras-Puente, A. Morales-Acevedo, G. Casados-Cruz, M.A. Hernandez-Perez, M.L. Albor-Aguilera, R. Mendoza-Perez, Rev. Mex. De Fis. 57 (2011) 441–445.
[23] F. Couzinie Devy1y, N. Barreau, J. Kessler, Prog. Photovolt. Res. Appl. 19 (2011) 527–536.
[24] B. Vidhya, S. Velumani, J.A. Arenas-Alatorre, Arturo Morales-Acevedo, R. Asomoza, J.A. Chavez-Carvayar, Mater. Sci. Eng. B 174 (2010) 216–221.
[25] B. Vidhya, S. Velumani, R. Asomoza, J. Nanopart. Res. 13 (2011) 3033–3042.
[26] S. Velumani, B.J. Babu, B. Vidhya, P. Reyes, A. Angeles, R. Asomoza, in: Proceedings of the 37th IEEE PVSC, 2011.
[27] B.J. Babu, S. Velumani, Arturo Morales-Acevedo, R. Asomoza, in: Proceedings of the 7th CCE, 2010, ISBN: 978-1-4244-7314-4.
[28] B.J. Babu, S. Velumani, R. Asomoza, in: Proceedings of the 37th IEEE PVSC, 2011.
[29] S. Roy, P. Guha, S.N. Kundu, H. Hanzawa, S. Chaudhuri, A.K. Pal, Mater. Chem. Phys. 73 (2002) 24–30.
[30] K.T. Ramakrishna Reddy, R.B.V. Chalapathy, Cryst. Res. Technol. 34 (1) (1999) 127–132.
[31] J. Bougnot, S. Duchemin, M. Savelli, Sol. cells 16 (1986) 221–236.
[32] D.Y. Lee, S. Park, J. Kim, Curr. Appl. Phys. 11 (2011) S88–S92.
[33] Subba Ramaiah Kodigala, Thin Films and Nanostructures Cu$(In_{1-x}Ga_x)Se_2$ Based Thin Film Solar Cells, Academic Press, 2010.
[34] M.B. Ard, K. Granath, L. Stolt, Thin Solid Films 361-362 (2000) 9–16.
[35] M.G. Faraj, K. Ibrahim, A. Salhin, Mater. Sci. Semicond. Process. 15 (2012) 206–213.
[36] D. Rudmann, G. Bilger, M. Kaelin, F.J. Haug, H. Zogg, A.N. Tiwari, Thin Solid Films 431-432 (2003) 37–40.
[37] K.L. Chopra, S.R. Das, Thin Film Solar Cells, Springer, New York, 1983.
[38] L. Zhang, Q. He, W.L. Jiang, F.F. Liu, C.J. Li, Y. Sun, Sol. Energy Mater. Sol. Cells 93 (2009) 114–118.
[39] B.J. Stanbery, S. Kincal, S. Kim, T.J. Anderson, O.D. Crisalle, S.P. Ahrenkiel, G. Lippold, in: Proceedings of the Twenty Eighth IEEE Photovoltaic Specialists Conference, 2000, pp. 440–445.
[40] D. Rudmann, Effects of Sodium on Growth and Properties of Cu(In Ga)Se_2 Thin Films and Solar Cells, , 2004 (Thesis).
[41] F.J. Haug, D. Rudmann, A. Romeo, H. Zogg, A.N. Tiwari, Electrical properties of the heterojunction in Cu(In,Ga)Se_2 superstrate solar cells, in: Proceedings of the 3rd World Conference on Photovoltaic Conversion, 2003.
[42] T.K. Todorov, O. Gunawan, T. Gokmen, D.B. Mitzi, Prog. Photovolt. Res. Appl. 21 (2013) 82–87.

Please cite this article as: B.J. Babu, et al., Materials Science in Semiconductor Processing (2015), http://dx.doi.org/10.1016/j.mssp.2015.01.002